

1
2
3
4
5

6
7
8
9
10
11
12
13
14
15
16
17
18
19
20
21
22
23
24

Towards narrowing uncertainty in future projections of local extreme precipitation

**Francesco Marra^{1,2,*}, Moshe Armon¹, Ori Adam¹, Davide Zoccatelli¹, Osama Gazal³,
Chaim I. Garfinkel¹, Dorita Rostkier-Edelstein^{1,4}, Uri Dayan⁵, Yehouda Enzel¹, and Efrat
Morin¹**

¹The Fredy and Nadine Herrmann Institute of Earth Sciences, The Hebrew University of
Jerusalem, Israel

²Institute of Atmospheric Sciences and Climate, National Research Council of Italy, CNR-ISAC,
Bologna, Italy

³Faculty of Agricultural and Environmental Sciences, Szent Istvan University, Hungary

⁴Department of Environmental Physics, Environmental Sciences Division, IIBR, Ness-Ziona,
Israel

⁵Department of Geography, The Hebrew University of Jerusalem, Israel

Corresponding author: Francesco Marra (f.marra@isac.cnr.it)

*Via Gobetti, 101, 40129, Bologna, Italy

Key Points:

- Local observations can be used to constrain the intensity distribution of precipitation events associated to different synoptic systems
- The constraints allow projecting extreme return levels at scales relevant for impact studies from synoptic information from climate models
- The approach improves the predictability of local extremes, independent of improvements in climate models at regional and local scales

25 **Abstract**

26 Projections of extreme precipitation based on modern climate models suffer from large
27 uncertainties. Specifically, unresolved physics and natural variability limit the ability of climate
28 models to provide actionable information on impacts and risks at the regional, watershed and city
29 scales relevant for practical applications. Here we show that the interaction of precipitating
30 systems with local features can constrain the statistical description of extreme precipitation.
31 These observational constraints can be used to project local extremes of low yearly exceedance
32 probability (e.g., 100-year events) using synoptic-scale information from climate models, which
33 is generally represented more accurately than the local-scales, and without requiring climate
34 models to explicitly resolve extremes. The novel approach offers a path for improving the
35 predictability of local statistics of extremes in a changing climate, independent of pending
36 improvements in climate models at regional and local scales.

37 **Plain Language Summary**

38 Climate change impact studies are currently restrained by the limited accuracy of climate models
39 in resolving precipitation extremes and by the uncertainties characterizing their analysis. We use
40 here a novel approach which permits to project extreme precipitation for future climatic
41 scenarios based on the combination of coarse-scale information from climate models with local
42 observations. Focusing on the south-eastern Mediterranean, we provide projections of
43 precipitation extremes which could not yet be derived using traditional methods, such as the
44 events occurring on average once in 100 years. The combined effect of changes in intensity and
45 average yearly number of two dominant synoptic systems is projected to increase the intensity of
46 the 100-year events in the coast and in the desert areas of the region, and to decrease it
47 elsewhere. The novel approach offers a path for improving the predictability of extremes in a
48 changing climate, independent of pending improvements in climate models.

49 **1 Introduction**

50 In recent decades, natural hazards associated with extreme precipitation, such as floods
51 and landslides, claimed thousands of lives and billions of US\$ in damages every year (NOAA,
52 2020; Paprotny et al., 2018). These numbers are expected to grow in response to an expansion of
53 population and wealth towards hazard-prone areas and to modifications in the hydrological cycle
54 induced by climate change (Ceola et al., 2014; Fischer and Knutti, 2016; Winsemius et al.,
55 2016). Quantifying climate change impact on extremes is thus a major challenge for the research
56 community (Blöschl et al, 2019). Hydrological design and risk management, particularly relevant
57 for adaptation efforts, require information on low *yearly* exceedance probabilities (Chow et al.,
58 1988), such as the events exceeded on average once in 100 years (hereon 100-year *return levels*,
59 with 1% yearly exceedance probability). To directly quantify return levels, long data series are
60 required, several times longer than the exceedance probability timescale. Since observational
61 records rarely exceed 50-100 years, some form of statistical extrapolation is generally required
62 (Coles, 2001).

63 Earth system models (ESMs) are commonly used to guide impact studies. However,
64 current ESMs are not able to explicitly resolve convective and microphysical processes critical
65 for precipitation extremes, and rely instead on parameterizations (Wilcox and Donner, 2007).
66 Additionally, their output is most relevant at scales which are too coarse for many practical
67 applications (Fischer et al., 2013; Hausfather et al., 2019). Dynamical downscaling methods can
68 provide projections for a region of interest, but are sensitive to the boundary conditions provided
69 by global models (Shepherd, 2014; Keller et al., 2018). Furthermore, their application is limited
70 by computational requirements so that, currently, only few regions are covered with 10-20-year
71 simulations (Kendon et al., 2014; Fosse et al., 2020), which are too short to reliably estimate 10-
72 years return levels, let alone 100-year events. Alternatively, statistical models are combined with
73 variables that are strongly related to extreme precipitation but more reliably reproduced in ESMs,
74 such as temperature (Snippel et al., 2015; Pfahl et al., 2017).

75 The methods currently adopted to quantify return levels, however, heavily rely on
76 extremes, such as the maxima values in each year or the values exceeding high thresholds
77 (Coles, 2001). As these are rare and subject to large uncertainties, the applicability of these
78 methods in a changing climate is limited (Serinaldi and Kilsby, 2015). In fact, stochastic climate
79 variability sets a lower bound on the uncertainty in observed and modelled extremes (Fatichi et
80 al., 2016). Reliable projections of extreme return levels for future climate scenarios thus
81 necessarily entail either intensive dynamical downscaling of ESMs with convection-permitting
82 models, or novel statistical approaches able to better exploit the available information.

83 It is shown here that the interaction of precipitating systems with local features, such as
84 coastlines or orography, can constrain the statistical description of precipitation intensity. These
85 constraints, derived from in-situ observations, permit predicting future extreme return levels at
86 the local-scales based on coarse-resolution global climate model projections, and without
87 requiring models to explicitly resolve the extremes.

88 **2 Study area and data**

89 The south-eastern Mediterranean is regarded as a climate change hotspot, highly
90 vulnerable to water scarcity and precipitation-induced hazards (Alpert et al., 2002; Giorgi, 2006).
91 Strong spatial gradients in precipitation climatology (Fig. S1 and S2 in the Supporting
92 Information) emerge from the interactions of two main types of precipitating systems with
93 coastline and orography (Diskin, 1970): (i) low-pressure systems moving inland along westerly
94 tracks (Mediterranean cyclones, hereon *Type-1*), and (ii) low-pressure systems mainly extending
95 from the south (active Red Sea troughs, *Type-2*). These are characterized by distinct spatial
96 patterns and both yield extreme precipitation amounts (Armon et al., 2018; Marra et al., 2019a).
97 ESMs predict substantial changes in the intensity and occurrence frequency of both systems

98 (Hochman et al., 2018a; Hochman et al., 2018b; Zappa et al., 2015), implying non-linear changes
99 in the compound extremes, which can be further complicated by local effects.

100 2.1 Precipitation data

101 Daily precipitation data, summed up to 6:00UTC, were provided by the Ministry of
102 Water and Irrigation of Jordan (97 stations between 1980-1981 and 2017-2018) and the Israel
103 Meteorological Service (>1300 stations between 1948-1949 and 2017-2018). Data from Israeli
104 stations flagged as missing, inaccurate, interpolated or obtained from multi-day accumulations
105 were excluded from the analysis. Jordanian data were supplied with no quality indicators; we
106 therefore rely on quality controls by the data provider. Separate records measured in proximity of
107 up to 1 km distance and 50 m elevation were merged. Records were organized by hydrologic
108 years (September 1 to August 31). For each station, years with more than 14 unavailable days
109 and records with less than 30 hydrological years were discarded. The final dataset consists of 459
110 stations (404 from Israel, 55 from Jordan, average spatial density of $\sim 1/75$ km⁻²) with 30-70
111 complete years of record (50.1 ± 13.3 years). Stationarity of the annual maxima at each station is
112 ensured using the Phillips and Perron (1988) test (5% significance level), indicating that the data
113 adequately represent extremes under present conditions.

114 2.2 Local groups of stations

115 Groups of stations in which distinct local features dominate the interaction with the
116 precipitating systems are identified using a *kmeans* clustering algorithm based on geographical
117 (latitude, longitude, elevation) and precipitation (average wet-day amount, and standard
118 deviation of the wet-day amounts) properties, without any direct use of extreme precipitation
119 properties or classification of the precipitating systems. The variables are normalized to zero-
120 mean equi-dispersed distributions; the algorithm is iterated 99 times to ensure stable results.
121 Following the Calinski and Harabasz (1974) criterion, six groups are obtained, roughly
122 identifiable as: mountains, northern coast, lowlands, coast, deserts west of the Dead Sea rift, and
123 deserts east of the rift. The last two groups are characterized by similar climatic conditions and
124 are likely separated primarily due to the geographical distance, although differences in other
125 aspects may exist, such as elevation and distance from the sea. These two groups, which are
126 sparsely populated (only 21 stations in one group), were merged. The classification used in the
127 analysis consists of five groups: mountains, northern coast, lowlands, coast, and deserts (Fig. 1a).

128 3 Methods

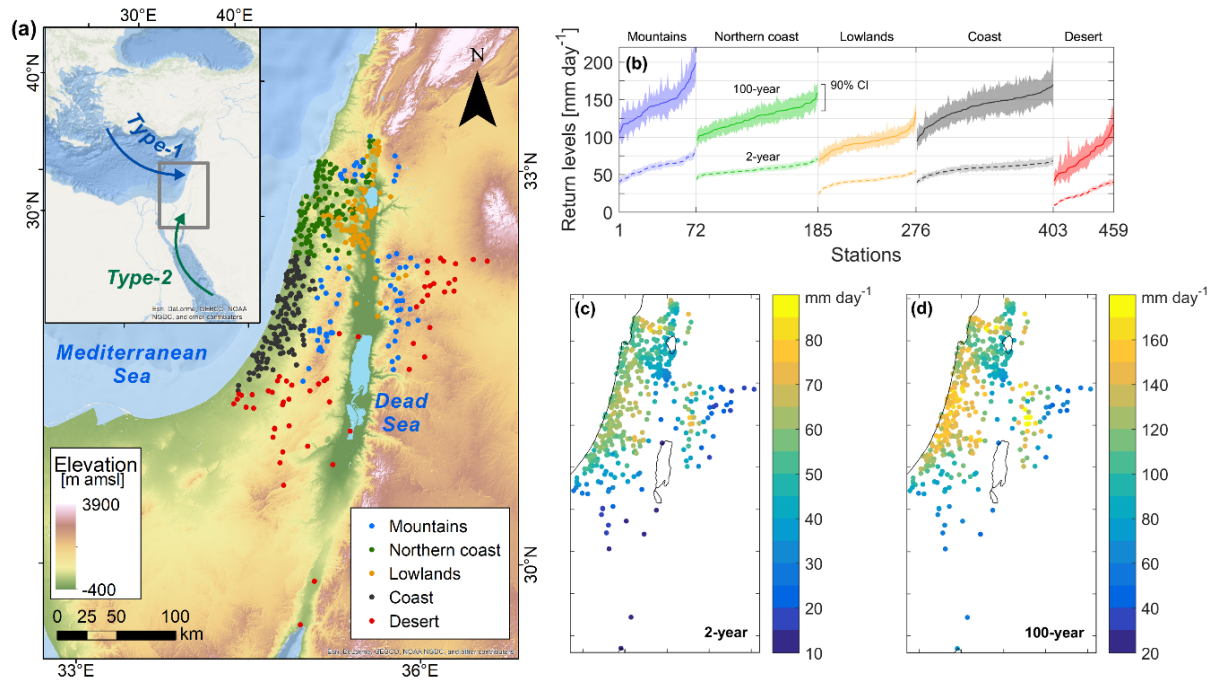
129 Extreme precipitation events were shown to emerge from underlying distributions of
130 ordinary events (Marani and Ignaccolo, 2015; Zorzetto et al., 2016), whose tails are generally
131 described by two parameters (e.g., stretched-exponential or power-type) (Cavanaugh et al., 2015;
132 Papalexiou et al., 2018; Marra et al., 2020b). By relying on ordinary events, for which more data
133 is available, this approach decreases the stochastic uncertainties inherent in the realization of
134 extremes (Zorzetto et al., 2016; Marra et al., 2018). Events generated by different types of

135 processes and thus described by distinct distributions such as mid-latitude vs. tropical cyclones
 136 (or, in our case, *Type-1* vs. *Type-2*) can be combined to derive a compound distribution for
 137 extreme return levels (Marra et al., 2019a; Miniussi et al., 2020). This distribution quantifies the
 138 yearly exceedance probability ζ associated with the precipitation amount x as a function of the
 139 intensity distributions of the ordinary events ($F_{i=1,\dots,S}$, where i represents the type of process) and
 140 the expected value of their yearly number of occurrences (n_i) such that: $\zeta(x) \simeq F_1^{n_1} \cdot F_2^{n_2} \cdot \dots \cdot$
 141 $F_S^{n_S}$ (Marra et al., 2019a). In this framework, changes in extreme return levels can be expressed
 142 as functions of the projected changes in the intensity distributions of the ordinary events and in
 143 the expected value of their yearly occurrences. While the occurrence frequency of synoptic
 144 events in the region can be resolved by ESMs (Hochman et al., 2018a; Cavicchia et al., 2020),
 145 precipitation intensity requires information on *two* degrees of freedom (i.e., the two parameters
 146 describing the distribution).

147 3.1 Ordinary events distributions and return levels

148 Ordinary events are defined as non-zero (i.e., ≥ 0.1 mm) daily precipitation amounts
 149 (Zorretto et al., 2016) associated with a precipitation type based on a semi-automatic, daily-
 150 based, synoptic classification (Alpert et al., 2004). Wet days corresponding to systems that are
 151 expected to be dry may have been wrongly classified; for example, synoptic conditions in the
 152 aftermath of Mediterranean cyclones are easily misinterpreted by the semi-automatic method.
 153 These were individually examined and labelled as *Type-1* if occurring up to 2 days after a *Type-1*
 154 day, and as *Type-2* in the remaining cases (Table S1).

155 Previous studies show that a Weibull distribution (stretched-exponential) in the form
 156 $F(x; \lambda, \kappa) = 1 - e^{-\left(\frac{x}{\lambda}\right)^\kappa}$, where λ is the scale and κ the shape parameter, well describes the tail of
 157 the two types of ordinary events in the region (Marra et al., 2019a). The shape parameter
 158 determines the tail heaviness, with heavier tails for smaller shapes and vice versa. These
 159 parameters are estimated left-censoring the lowest 75% of the observations while keeping their
 160 weight in probability, and using a least-square linear regression in Weibull-transformed
 161 coordinates (Marra et al., 2019a). The left-censoring prevents contaminations from the lower tail
 162 of the distribution, which may require more general formulations (Papalexiou et al., 2018;
 163 Cavanaugh et al., 2015) and is sensitive to the accuracy of the measurement device (Marra et al.,
 164 2019a). After left-censoring, the number of data points used for the parameter estimation in each
 165 of the stations is 426 ± 175 for *Type-1* (minimum 66), and 153 ± 68 (minimum 30) for *Type-2*.
 166 The expected number of yearly ordinary events is computed, for each type, as the mean of the
 167 yearly number of wet days. Extreme return levels are computed numerically by inverting the
 168 formulation $\zeta(x) \simeq F_1^{n_1} \cdot F_2^{n_2}$. Sample uncertainty in parameters and return levels is quantified
 169 via bootstrap with replacement (10^3 repetitions) among the years in the record (Overeem et al.,
 170 2008). The resulting return levels (Fig. 1; Fig. S2) are consistent with traditional methods based
 171 on the observed annual maxima (Fig. S3), but have significantly smaller uncertainty (22%, as
 172 opposed to 39%, median uncertainty on 100-year return levels).



173

174

175

176

177

178

179

180

181

182

183

Figure 1. Extremes emerge from the interaction of precipitation systems with local features. (a) Map of the study region showing the local terrain elevation, the main precipitating systems tracks, and the location of the daily precipitation stations used in the study, coloured according to groups in which different local features dominate the interaction with the precipitating systems. (b) Distribution of 2-year and 100-year return levels (50% and 1% yearly exceedance probability, respectively) of the five groups shown in panel a (with matching colours) displayed as transposed cumulative distributions. The respective uncertainty (shading) is calculated as the 90% confidence interval from 10^3 bootstrap samples with replacement among the years in the record. The median uncertainty across all groups is 14% (22%) for 2-year (100-year) return levels. (c, d) Map of the 2-year (c) and 100-year (d) return levels (colours indicate daily precipitation intensity).

184

3.2 Local constraints of the intensity distributions

185

186

187

188

189

190

191

192

193

194

195

196

A robust relationship between the scale λ and shape κ parameter of the ordinary events distributions would reduce the representation of precipitation intensity to *one* degree of freedom, enabling us to provide projections of extremes based only on changes in the mean intensity of ordinary events. The significance of the relationship between the parameters describing the two types of ordinary events at each of the five groups of stations is tested using the rank correlation (10^4 Monte Carlo reshuffling realizations). The coefficient α of the relations in the form $\kappa = \alpha \cdot \log \lambda + C$ is derived for each of the five groups and the two event types using a linear regression model based on a χ^2 minimization and considering parameter estimation errors in a Monte Carlo framework (10^3 realizations).

The coefficients α , calculated for each group, represent the local constraints on the intensity distribution. Higher α implies a stronger decrease in tail heaviness in response to an increase in the median intensity, and vice versa. Under these constraints the distribution has one

197 degree of freedom, meaning that any quantity not orthogonal to the constraint (e.g., mean,
 198 median, standard deviation, etc.) is sufficient to describe the distribution. Here, we use the
 199 median intensity, hereon denoted I , as it is less sensitive than the mean to the stochastic
 200 uncertainty in the realization of extremes: $F_i(x; \lambda_i, \kappa_i) = F(x; I_i)$. The return level x associated
 201 with the yearly exceedance probability p can be written as a function of median intensity and
 202 expected number of yearly occurrences of the two types of ordinary events by inverting the
 203 extreme value distribution $\zeta(x)$: $x(p) = \zeta^{(-1)}(p; I_1, n_1; I_2, n_2)$.

204 We assume that temporal changes in the distribution of ordinary events will preserve
 205 these local observational constraints. This resembles the assumptions behind regionalization
 206 approaches in which spatial information is traded for record length (Buishand, 1991), but extends
 207 its meaning in that (i) temporal changes are allowed, and (ii) the information on the interaction
 208 between precipitating systems and local features provided by each individual station is fully
 209 exploited (e.g. Marra et al., 2020a). To support our assumption, we test the significance of the
 210 constraints in historical observations in a Monte Carlo framework by examining groups of non-
 211 consecutive years with consistently different median intensity (see Fig. S4) along the following
 212 steps: (1) at each station and precipitation type, years are ranked according to the median
 213 ordinary events intensity; (2) six 5-year subsets of non-consecutive years are created by selecting
 214 three groups (15 years) from the largest intensity years and three from the smallest intensity; (3)
 215 Weibull parameters are estimated at each station for the 5-year subsets; (4) 10^3 m -elements
 216 synthetic samples, where m is the number of wet-days in the observed 5-year subsets, are
 217 generated according to the obtained distributions and the parameters describing the samples are
 218 estimated to quantify the impact of parameter estimation uncertainty; (5) logarithmic relations
 219 between the parameter pairs are derived for each subset; (6) the α coefficient representing the
 220 local constraint is compared to the distribution of coefficients of the logarithmic relations at (5).

221 3.3 Climate projections

222 Projected changes in median intensity and expected number of yearly occurrences of the
 223 two precipitation types are obtained by examining the difference between the ends of the 21st
 224 century (~2080-2100) and the 20th century (~1980-2005) under the RCP8.5 emission scenario
 225 (Riahi et al., 2011). We estimated these differences using the data presented in Hochman et al.
 226 (2018a) and Zappa et al. (2015), calculated for 8 and 17 CMIP5 models, respectively. We choose
 227 the changes in occurrence and median intensities from these two studies, as they are produced for
 228 the desired time period and emission scenario, and because these parameters are considered more
 229 robust than the changes in extremes that can be derived from the CMIP5 models themselves
 230 (Fatichi et al., 2016). In particular, the changes in synoptic circulation over the study region
 231 derived from CMIP5 ensembles were shown to be robust (Hochman et al., 2017; Hochman et al.,
 232 2018a; Zappa et al., 2015).

233 The acquired changes we used are: *Type-1*: expected number of yearly occurrence is
 234 projected to decrease by 15-35% (-25 ± 10 %); median intensity is projected to decrease by 20-
 235 25% ($+22.5 \pm 5$ %); *Type-2*: expected number of yearly occurrence is projected to increase by

236 13% ($+13 \pm 5$ %); annual *Type-2* precipitation amounts are projected to remain unchanged,
237 which leads to a 12% decrease in the median intensity (-12 ± 5 %). These numbers result in a
238 20-30% decrease in mean annual precipitation, which is consistent with the AR5 IPCC report
239 (IPCC, 2014). As based on relative differences between historic and future simulations, we
240 expect these projections to be less sensitive to systematic biases in the quantification of wet days
241 from CMIP5 models (e.g., too many drizzle days).

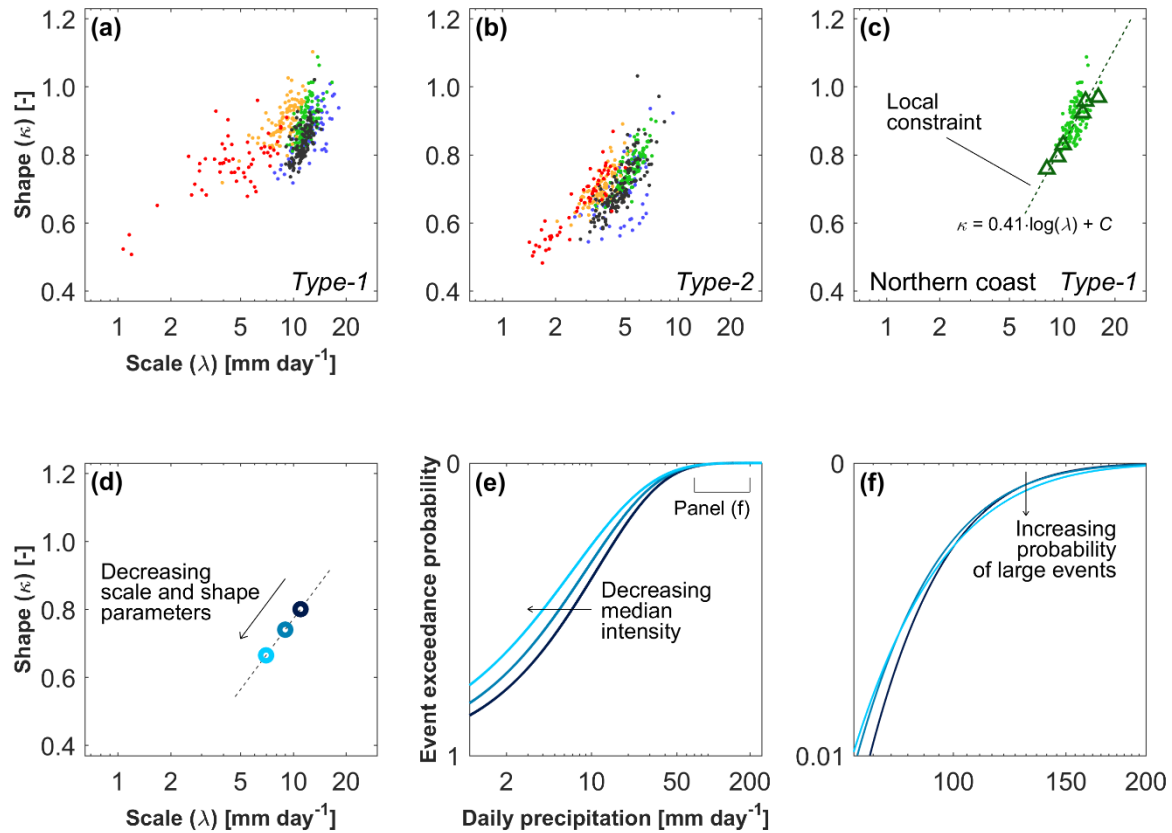
242 Changes in extreme return levels are computed in a Monte Carlo framework considering
243 uncertainties in the projections and in the local constraints (i.e., the α coefficients), as follows.
244 At each station, 10^3 projections are created by (1) sampling the projected change in number and
245 median intensity of the two ordinary events types from normal distributions, and (2) sampling
246 the α coefficient of the local constraint relations from the Monte Carlo realizations. Note that,
247 since the ratio between median and mean of Weibull distributions smoothly depends on the
248 shape parameter κ and is independent from the scale λ , one can safely assume a one-to-one
249 correspondence between projected changes in the mean and in the median (e.g., a 5% change in
250 the mean corresponds to $\sim 5\%$ change in the median). This is useful since the median is a better
251 descriptor for observed data whereas the mean is commonly provided by ESMs output.

252 **4 Application to the south-eastern Mediterranean**

253 4.1 Local constraints on the distribution of ordinary events

254 While relations between scale λ and shape κ parameters of the ordinary events
255 distributions are not expected *a priori*, statistically significant relations ($>3\sigma$ significance level)
256 are found for the given data when focusing on local groups of stations in which distinct local
257 features dominate the interactions with precipitation systems (Fig. 2a-c; Fig. S4). Dependence of
258 the form $\kappa = \alpha \cdot \log \lambda + C$, where α and C are empirically-determined, was found to
259 approximate these relations in each group, generally explaining most of the observed variance
260 (Fig. S4). The hypothesis of a local constraint α being significantly different from the
261 coefficients obtained from temporally splitting the records is rejected in all the cases (5%
262 significance level). Thus, the local values of α indeed reflect historical changes in the median
263 intensity of ordinary events at each station, supporting the validity of the approach under
264 changing conditions (Fig. 2c; Fig. S4). It is worth noting that these relations are based on
265 historical observations and thus comprise observed changes in both dynamics and
266 thermodynamics.

267 The observed constraints imply that changes in the median intensity are linked to
268 contrasting changes in extremes, i.e., decreasing median intensity decreases the precipitation
269 amount yielded by typical ordinary events (Fig. 2d, e) but increases the probability associated
270 with the largest events, and *vice versa* (Fig. 2f). This counter-intuitive behaviour is consistent
271 with previous theory and observations of extreme precipitation, and supports the local constraints
272 approach as a framework for quantifying changes in extremes (O’Gormann and Schneider, 2009;
273 Pendergrass, 2018; Pendergrass and Knutti, 2018; Myhre et al., 2019; Wasko et al., 2018).



274

275

276 **Figure 2.** Local constraints on the intensity distribution of ordinary precipitating events. (a, b) Scatter277 plots of the shape (κ) and scale (λ) parameters of the observed distributions for the two types of ordinary278 events; colours refer to the five groups of stations as in Fig. 1a. (c) Example of the local constraint (*Type-*279 *1*, northern coast); triangles represent the median (among stations) parameters obtained in the split-sample

280 test using, for each station, groups of five non-consecutive years with increasing median intensity of the

281 ordinary events; triangles thus represent historical variations of intensity. Local constraints for all cases

282 are shown in Fig. S4. (d) Schematic of the projection of changes in the intensity distribution of the

283 ordinary events along the constraints ($\alpha = 0.3$, $\lambda = 11.0, 9.0, 7.0$ mm day⁻¹ and $\kappa = 0.8, 0.74, 0.66$;

284 black, blue and cyan, respectively); (e) event exceedance probability distributions associated with the

285 three pairs of scale and shape parameters shown in (d); (f) the largest 1% of the events in these

distributions.

286

4.2 Projections of future extremes

287

288 The sensitivity of extreme return levels to changes in the ordinary events (Fig. S5; Fig.

289 S6) highlights that different return levels can have different responses, and that the local

290 sensitivities associated with each event type can differ significantly. For example, in most of the

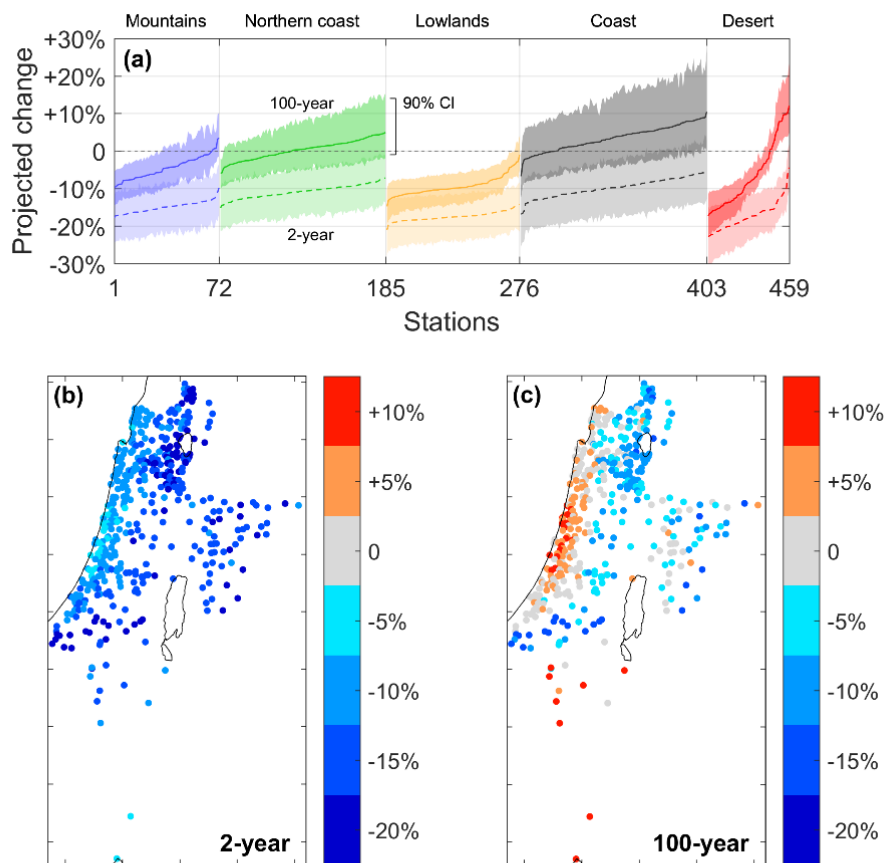
291 region return levels are tied to changes in intensity and number of *Type-1* events, while changes292 in *Type-2* are crucial drivers for extreme return levels in the desert areas (Fig S5). Local changes

293 in extreme return levels are thus related to mean (or median) changes in precipitation in a

complex manner.

294 The projected changes in occurrence frequency of the two types (25% decrease and 13%
 295 increase, respectively) and intensity (20-25% and 12% decrease, respectively), yield the changes
 296 in the extreme return levels shown in Fig. 3 (see Fig. S7 for more details). An overall 5-20%
 297 decrease of the 2-year return levels is seen, driven by the decrease in the occurrence frequency of
 298 Mediterranean cyclones and in the median intensity of both types of systems. Since in the
 299 climatological setting of the region 2-year return levels roughly correspond to 99th wet-day
 300 percentiles, this is consistent with previous results based on downscaling methods (Hochman et
 301 al, 2018b). The picture is drastically different for the 100-year return levels which could not be
 302 assessed in previous studies. Along the coast and in the southern desert, the negative sensitivity
 303 to changes in the median intensity (Fig. S5; Fig. S6) dominates, and the rarest extremes are
 304 projected to increase, consistently with Fig 2f. These results imply two adverse effects: (i)
 305 amplified water scarcity and reduced flood and landslide risks in most of the region (Alpert et al.,
 306 2002; Samuels et al., 2009; Peleg et al., 2015); and (ii) increased intensity of the most severe
 307 events along the coast and southern deserts, associated with augmented risk of extreme pluvial
 308 flooding in coastal cities, and of flash floods, debris flows and geomorphic responses in the
 309 southern deserts (Shmilovitz et al., 2020; Rinat et al., 2020).

310



311

312 **Figure 3.** Projected changes in extreme precipitation return levels. Projected changes in 2-year and 100-
 313 year return levels (50% and 1% yearly exceedance probability, respectively) for the end of the century

314 (difference between ~2080-2100 and ~1980-2005) under the RCP8.5 emission scenario. (a) Distribution
315 of the projected change and relative uncertainty (90% confidence interval considering uncertainties both
316 in climate projections and local constraints) shown as transposed cumulative distributions; colours refer to
317 the five groups of stations as in Fig. 1a. (b-c) Map of the projected changes for the 2-year (b) and 100-
318 year (c) return levels.

319 **5 Discussion and conclusions**

320 In the south-eastern Mediterranean, the dominance of two precipitating systems and the
321 availability of high-density local data makes it possible to simplify the statistical description of
322 ordinary precipitation events, and therefore of extreme events that emerge as the tails of their
323 distributions. Previous studies on the water resources of the region projected a “less rainfall,
324 more extremes” situation, with increased extremes insufficient to impact water resources in
325 generally drying conditions. However, these previous studies could not quantify changes in
326 extreme return levels and therefore risk (Alpert et al., 2002; Peleg et al., 2015). Combining
327 information on the occurrence frequency and intensity of the two dominant precipitation types
328 from ESM projections and observational constraints from rain stations, we show that the changes
329 in extreme return levels strictly depend on the sought probability. A tendency towards a general
330 decrease in the intensity of the 2-year events is found, together with an increase of the most
331 severe (100-year) events along the coast and in the desert areas.

332 The robustness of the synoptic variations in the RCP8.5 scenario in the region (Hochman
333 et al., 2018a; Zappa et al., 2015) and of the local constraints (Fig. S6), demonstrate the reliability
334 of the proposed approach and the local projected response. Nevertheless, our predictions may be
335 refined by analysing additional scenarios and local data. It is plausible that similar improvements
336 in the projection of extremes can be made in other regions, even though projected changes in the
337 synoptic circulation systems might be less robust (Shepherd, 2014), calling for specific efforts to
338 narrow this source of uncertainty. Additionally, future climate might reach some tipping point
339 after which the observational local constraints may no longer hold, a possibility that could be
340 tested using long simulations from convection-permitting models. For example, new synoptic
341 systems could be introduced in the region (such as tropical-like cyclones), or the track of existing
342 systems could change to such a degree that the interactions with local features might change
343 substantially, thus deviating from the observed constraints (e.g. northward shift of Mediterranean
344 cyclones track). Our results, which pertain to daily precipitation, assume no change in the spatial
345 structure of precipitation events at scales smaller than the resolutions of the used climate models.
346 Improvements in the statistical description of the precipitating systems at multiple temporal and
347 spatial scales derived from observations and/or convection permitting models could fill this gap
348 by quantifying their structural response to external forcing (Cannon and Innocenti, 2019; Wasko
349 et al., 2016; Peleg et al., 2018; Marra et al., 2020b).

350 In contrast to traditional methods, the local constraints approach does not require long
351 records; rather, it only requires local observations of ordinary events to constrain the intensity
352 distributions. To this end, remotely sensed precipitation datasets represent a promising source of
353 information for ungauged areas (Marra et al., 2019b). While uncertainty in ESMs remains a

354 significant challenge to the community (Palmer and Stevens, 2019), our results point to increased
355 investment in local measurements as an actionable and promising path to reduced uncertainty in
356 the projection of extremes, independent of climate modelling efforts.

357 The framework can be extended to other processes whose extremes emerge from
358 underlying distributions of ordinary events, such as extremes emerging from the combination of
359 different physical phenomena, e.g. winds and storm surges from different types of cyclones
360 (Miniussi et al., 2020; Cavicchia et al., 2020). Similarly, it can be applied to phenomena whose
361 intensity and occurrence may change independently, e.g. occurrence and maximum lifetime
362 intensity of tropical cyclones (Knutson et al., 2010). In regions where local constraints can be
363 obtained, the approach proposed here can improve the predictability of climate change impact on
364 extremes at scales relevant for impact studies, whose uncertainty was previously considered
365 irreducible due to modelling uncertainty and natural variability.

366 **Acknowledgements**

367 The authors declare no conflict of interests. Precipitation data were provided by Israel
368 Meteorological Service (<https://ims.gov.il/en>, September 2018; data is freely available in Hebrew
369 only) and Ministry of Water and Irrigation of Jordan, Technical Affairs, Studies Directorate,
370 Hydrological and Meteorological Information Systems (rainfall stations archives files, October
371 2018; available upon request to the data providers). The authors thank Prof. Pinhas Alpert for the
372 synoptic classification. Data and codes supporting the results are available at:
373 <https://doi.org/10.5281/zenodo.4286160> and <https://doi.org/10.5281/zenodo.3971558>. The linear
374 fit with uncertainty in x and y was performed based on the function by J. Browaeys, MATLAB
375 Central File Exchange ([https://www.mathworks.com/matlabcentral/fileexchange/45711-linear-](https://www.mathworks.com/matlabcentral/fileexchange/45711-linear-fit-with-both-uncertainties-in-x-and-in-y)
376 [fit-with-both-uncertainties-in-x-and-in-y](https://www.mathworks.com/matlabcentral/fileexchange/45711-linear-fit-with-both-uncertainties-in-x-and-in-y), retrieved March 25, 2020). This study was funded by
377 the Israel Ministry of Science and Technology [grant no. 61792], Israel Science Foundation
378 [grant no. 1069/18], NSF-BSF [grant no. BSF 2016953], JNF [grant no. 90-01-550-18] and
379 Google [gift grant]. It is a contribution to the HyMeX program. Authors contribution:
380 Conceptualization: FM, MA, OA, DZ, EM; Formal analyses: FM; Data curation: FM, OG;
381 Funding acquisition: EM, OA, CG, UD, DRE, YE; Paper writing: FM; Paper review and editing:
382 all authors.

383 **References**

- 384 Alpert P *et al* 2002 The paradoxical increase of mediterranean extreme daily rainfall in spite of
385 decrease in total values. *Geophys. Res. Lett.* **29(11)**, 31
- 386 Alpert P, Osetinsky I, Ziv B, Shafir H 2004 Semi-Objective Classification for Daily Synoptic
387 Systems: Application to the Eastern Mediterranean Climate Change. *Int. J. Climatol.* **24(8)**,
388 1001–11
- 389 Armon M, Dente E, Smith JA, Enzel Y, Morin E 2018 Synoptic-scale control over modern
390 rainfall and flood patterns in the levant drylands with implications for past climates. *J.*
391 *Hydrometeorol.* **19**, 1077–1096

- 392 Benestad RE, Nychka D, Mearns LO 2012 Spatially and temporally consistent prediction of
393 heavy precipitation from mean values. *Nature Clim. Change* **2**, 544-547
- 394 Blöschl G *et al* 2019 Twenty-three unsolved problems in hydrology (UPH) – a community
395 perspective. *Hydrol. Sci. J.* **64(10)**, 1141–1158
- 396 Buishand, T.A., 1991. Extreme rainfall estimation by combining data from several sites. *Hydrol.*
397 *Sci. J.*, **36 (4)**, 345–365, doi:10.1080/0262666910949251
- 398 Calinski T, Harabasz JA 1974 dendrite method for cluster analysis. *Comm. Stat.* **3(1)**, 1–27
- 399 Cannon AJ, Innocenti S 2019 Projected intensification of sub-daily and daily rainfall extremes in
400 convection-permitting climate model simulations over North America: implications for future
401 intensity–duration–frequency curves. *Nat. Hazards Earth Syst. Sci.* **19**, 421–440
- 402 Cavanaugh NR, Gershunov A, Panorska AK, Kozubowski TJ 2015 The probability distribution
403 of intense daily precipitation. *Geophys. Res. Lett.* **42**, 1560–1567
- 404 Cavicchia L, Pepler A, Dowdy A, Evans J, Di Luca A, Walsh K 2020 Future changes in the
405 occurrence of hybrid cyclones: The added value of cyclone classification for the east
406 Australian low-pressure systems. *Geophys. Res. Lett.* **47**, e2019GL085751
- 407 Ceola S, Laio F, Montanari A 2014 Satellite Night Time Lights Reveal Increasing Human
408 Exposure to Floods Worldwide *Geophys. Res. Lett.* **41(20)**, 7184–90
- 409 Chow VT, Maidment DR, Mays LW 1988 *Applied Hydrology*, McGraw-Hill
- 410 Coles S 2001 *An Introduction to Statistical Modeling of Extreme Values*, Springer-Verlag,
411 London
- 412 Diskin MH 1970 Factors affecting variations of mean annual rainfall in Israel. *Int. Ass. Sci.*
413 *Hydrol. Bull.* **15:4**, 41-49
- 414 Fatichi S, Ivanov VY, Paschalis A, Peleg N, Molnar P, Rimkus S, Kim J, Burlando P, Caporali E
415 2016 Uncertainty partition challenges the predictability of vital details of climate change.
416 *Earth's Future* **4(5)**, 240-251
- 417 Fischer EM, Knutti R 2016 Observed heavy precipitation increase confirms theory and early
418 models. *Nat. Clim. Change* **6**, 986-991
- 419 Fischer EM, Beyerle U, Knutti R 2013 Robust spatially aggregated projections of climate
420 extremes. *Nat. Clim. Change* **3**, 1033–1038
- 421 Fossier, G., Kendon, E. J., Stephenson, D., & Tucker, S. (2020). Convection-permitting models
422 offer promise of more certain extreme rainfall projections. *Geophys. Res. Lett.*, **47**,
423 e2020GL088151
- 424 Giorgi F 2006 Climate change Hot-spots. *Geophys. Res. Lett.* **33**, L08707
- 425 Hausfather Z, Drake HF, Abbot T, Schmidt GA 2019 Evaluating the Performance of Past
426 Climate Model Projections, *Geophys. Res. Lett.* **47**, e2019GL085378
- 427 Hochman A, Harpaz T, Saaroni H, Alpert P 2018a Synoptic classification in 21st century CMIP5
428 predictions over the Eastern Mediterranean with focus on cyclones. *Int. J. Climatol.* **38**, 1476-
429 1483

- 430 Hochman A, Mercogliano P, Alpert P, Saaroni H, Bucchignani E 2018b High-resolution
431 projection of climate change and extremity over Israel using COSMO-CLM. *Int. J. Climatol.*
432 **38(14)**, 5095-5106
- 433 IPCC 2014 *Climate Change 2014: Synthesis Report. Contribution of Working Groups I, II and*
434 *III to the Fifth Assessment Report of the Intergovernmental Panel on Climate Change*, Core
435 Writing Team, R.K. Pachauri and L.A. Meyer eds. IPCC, Geneva, Switzerland
- 436 Keller M, Kroner N, Fuhrer O, Luthi D, Schmidli J, Stengel M, Stockli R, Schar C 2018 The
437 sensitivity of alpine summer convection to surrogate climate change: An intercomparison
438 between convection-parameterizing and convection-resolving models, *Atmos. Chem. Phys.*
439 **18(8)**, 5253–5264
- 440 Kendon EJ, Roberts NM, Fowler HJ, *et al* 2014 Heavier summer downspours with climate
441 change revealed by weather forecast resolution model. *Nat. Clim. Change*. **4**, 570-576
- 442 Knutson TR *et al* 2010 Tropical cyclones and climate change. *Nat. Geosci.* **3**, 157-163
- 443 Marani M, Ignaccolo M 2015 A metastatistical approach to rainfall extremes. *Adv. Water*
444 *Resour.* **79**, 121–126
- 445 Marra F, Armon M, Borga M, Morin E 2020a Orographic effect on extreme precipitation
446 statistics peaks at hourly time scales. Under review. *Preprint available at*
447 *doi:10.1002/essoar.10504622.1*
- 448 Marra F, Borga M, Morin E 2020b A Unified Framework for Extreme Sub-daily Precipitation
449 Frequency Analyses based on Ordinary Events. *Geophys. Res. Lett.*, **47**, e2020GL090209
- 450 Marra F, Nikolopoulos EI, Anagnostou EN, Bárdossy A, Morin E 2019b Precipitation frequency
451 analysis from remotely sensed datasets: A focused review. *J. Hydrol.* **574**, 699-705
- 452 Marra F, Nikolopoulos EI, Anagnostou EN, Morin E 2018 Metastatistical Extreme Value
453 analysis of hourly rainfall from short records: Estimation of high quantiles and impact of
454 measurement errors. *Adv. Water Resour.* **117**, 27-39
- 455 Marra F, Zoccatelli D, Armon M, Morin E 2019a A simplified MEV formulation to model
456 extremes emerging from multiple nonstationary underlying processes. *Adv. Water Resour.*
457 **127**, 280-290
- 458 Miniussi A, Villarini G, Marani M 2020 Analyses through the Metastatistical Extreme Value
459 distribution identify contributions of Tropical Cyclones to rainfall extremes in the Eastern US.
460 *Geophys. Res. Lett.* **47**, e2020GL087238
- 461 Myhre G *et al* 2019 Frequency of extreme precipitation increases extensively with event rareness
462 under global warming. *Sci. Reports* **9**, 16063
- 463 NOAA, 2020 U.S. billion-dollar weather and climate disasters. NCEI,
464 <https://www.ncdc.noaa.gov/billions/summary-stats>
- 465 O’Gorman PA, Schneider T 2009 The physical basis for increases in precipitation extremes in
466 simulations of 21st-century climate change. *Proc. Natl. Acad. Sci. U. S. A.*, **106(35)**, 14773-
467 14777
- 468 Overeem A, Buishand A, Holleman I 2008 Rainfall depth-duration-frequency curves and their
469 uncertainties. *J. Hydrol.* **348**, 124–134

- 470 Palmer T, Stevens B 2019 The scientific challenge of understanding and estimating climate
471 change. *Proc. Natl. Acad. Sci. U. S. A.* **116(49)**, 24390-24395
- 472 Papalexiou SM, AghaKouchak A, Foufoula-Georgiou E 2018 A diagnostic framework for
473 understanding climatology of tails of hourly precipitation extremes in the United States.
474 *Water Resour. Res.* **54**, 6725–6738
- 475 Paprotny D, Sebastian A, Morales-Napoles O, Jonkman SN 2018 Trends in flood losses in
476 Europe over the past 150 years. *Nat. Comm.* **9**, 1985
- 477 Peleg N, Marra F, Fatichi S, Molnar P, Morin E, Sharma A, Burlando P 2018 Intensification of
478 convective rain cells at warmer temperatures observed from high-resolution weather radar
479 data. *J. Hydrometeorol.* **19**, 715-726
- 480 Peleg N, Shamir E, Georgakakos KP, Morin E 2015 A framework for assessing hydrological
481 regime sensitivity to climate change in a convective rainfall environment: a case study of two
482 medium-sized eastern Mediterranean catchments, Israel *Hydrol. Earth Syst. Sci.* **19**, 567–581
- 483 Pendergrass AG 2018 What precipitation is extreme? *Science* **360**, 6393
- 484 Pendergrass AG, Knutti R 2018 The uneven nature of daily precipitation and its change.
485 *Geophys. Res. Lett.* **45**, 11980–11988
- 486 Pfahl S, O’Gorman PA, Fischer EM 2017 Understanding the regional patten of projected future
487 changes in extreme precipitation. *Nat. Clim. Change* **7**, 423-428
- 488 Phillips P, Perron P 1988 Testing for a Unit Root in Time Series Regression. *Biometrika* **75**,
489 335–346
- 490 Riahi K, Rao S, Krey V, Cho C, Chirkov V, Fischer G, Kindermann G, Nakicenovic N, Rafaj P
491 2011 RCP 8.5 – A scenario of comparatively high greenhouse gas emissions. *Clim. Change*
492 **109**, 33-57
- 493 Rinat Y, Marra F, Armon M, Metzger A, Levi Y, Khain P, Vadislavsky E, Rosensaft M, Morin E
494 2020 Hydrometeorological analysis and forecasting of a 3-day flash-flood-triggering desert
495 rainstorm, *Nat. Hazards Earth Syst. Sci. Discuss.*, Under review, Preprint available at
496 doi:10.5194/nhess-2020-189
- 497 Samuels R, Rimmer A, Alpert P 2009 Effect of extreme rainfall events on the water resources of
498 the Jordan River. *J. Hydrol.* **375**, 513-523
- 499 Schär C *et al* 2016 Percentile indices for assessing changes in heavy precipitation events. *Clim.*
500 *Change* **137**, 201-216
- 501 Serinaldi F, Kilsby CG 2015 Stationarity is undead: Uncertainty dominates the distribution of
502 extremes. *Adv. Water Resour.* **77**, 17-36
- 503 Shepherd TG 2014 Atmospheric circulation as a source of uncertainty in climate change
504 projections. *Nat. Geosci.* **7**, 703–708
- 505 Shmilovitz Y, Morin E, Rinat Y, Haviv I, Carmi G, Mushkin A, Enzel Y 2020 Linking
506 frequency of rainstorms, runoff generation and sediment transport across hyperarid talus-
507 pediment slopes. *Earth Surf. Proc. Landforms* **49(7)**, 1644-1659

- 508 Sippel S, Mitchell D, Black MT, Dittus AJ, Harrington L, Schaller N, Otto FEL 2015 Combining
509 large model ensembles with extreme value statistics to improve attribution statements of rare
510 events. *Weather Clim. Extremes* **9**, 25-35
- 511 Wasko C, Lu WT, Mehrotra R 2018 Relationship of extreme precipitation, dry-bulb temperature,
512 and dew point temperature across Australia. *Env. Res. Lett.* **13**, 074031
- 513 Wasko C, Sharma A, Westra S 2016 Reduced spatial extent of extreme storms at higher
514 temperatures. *Geophys. Res. Lett.* **43**, 4026–4032
- 515 Wilcox EM, Donner LJ 2007 The frequency of extreme rain events in satellite rain-rate estimates
516 and an atmospheric general circulation model. *J. Climate* **20**, 53–69
- 517 Winsemius HC *et al* 2016 Global drivers of future river flood risk. *Nat. Clim. Change* **6**, 381-385
- 518 Zappa G, Hawcroft MK, Shaffrey L, Black E, Brayshaw DJ 2015 Extratropical cyclones and the
519 projected decline of winter Mediterranean precipitation in the CMIP5 models. *Clim. Dyn.*
520 **45(7–8)**, 1727–1738
- 521 Zorzetto E, Botter G, Marani M 2016 On the emergence of rain- fall extremes from ordinary
522 events. *Geophys. Res. Lett.* **43**, 8076–8082